

Sodium and potassium intercalation into Ta<sub>2</sub>PdS<sub>6</sub>

P.A. Hyde, S.J. Clarke\*

Department of Chemistry, University of Oxford, Inorganic Chemistry Laboratory, South Parks Road, Oxford, OX1 3QR, UK

## ARTICLE INFO

## Keywords:

Intercalation

Transition metal chalcogenides

Narrow band gap semiconductor

## ABSTRACT

Two new phases derived from the layered ternary chalcogenide Ta<sub>2</sub>PdS<sub>6</sub> have been successfully synthesised via the intercalation of sodium or potassium. MTa<sub>2</sub>PdS<sub>6</sub> (M = Na, K) crystallise in monoclinic space group *I2/m* (No. 12), *Z* = 2, with lattice parameters *a* = 8.1366(7) Å, *b* = 3.2876(1) Å, *c* = 15.3279(3) Å, β = 97.407(2)° for NaTa<sub>2</sub>PdS<sub>6</sub>, and *a* = 8.3845(3) Å, *b* = 3.2955(1) Å, *c* = 16.7416(8) Å, β = 86.339(3)° in the case of KTa<sub>2</sub>PdS<sub>6</sub>. The general structure of the parent phase is retained upon intercalation, with increased unit cell volumes of 17.3% and 33.2% for the Na and K intercalates respectively. SQUID magnetometry shows that both intercalates are net diamagnets, but shows a significant reduction of magnetic susceptibility from Ta<sub>2</sub>PdS<sub>6</sub> due to the increase in a Pauli paramagnetic component due to partial band filling.

## 1. Introduction

Layered transition metal chalcogenides have experienced a recent resurgence in popularity due to their unusual physical properties arising from their low dimensionality, a consequence of the polarisability of the chalcogenide ion [1]. Due to the development of air-sensitive techniques and improved characterisation methods, a surge in synthesis of ternary chalcogenides occurred in the 1980's [2–9]. The layered structure of many of these compounds make them ideal candidates for intercalation which can cause dramatic changes to their physical properties. Intercalation of Li into TiS<sub>2</sub> was used as a prototypical secondary battery system [10] and Li and NH<sub>3</sub> intercalation into FeSe has shown to increase the superconducting *T*<sub>c</sub> to about 45 K [11].

Ta<sub>2</sub>PdCh<sub>6</sub> (Ch = S, Se), first synthesised in 1985, are also members of the ternary transition-metal chalcogenide family. Both compounds are isostructural and crystallise in space group *I2/m* (No. 12) with lattice parameters *a* = 9.960(13) Å, *b* = 3.271(5) Å, *c* = 11.696(16) Å, β = 114.51(4)° and *a* = 10.423(6) Å, *b* = 3.375(2) Å, *c* = 12.196(6) Å, β = 113.68(2)° for the sulfide and selenide respectively [3]. Each layer consists of chains of face-sharing monocapped triangular prismatic TaCh<sub>7</sub> units bridged by square planar PdCh<sub>4</sub> units. Electrical conductivity measurements supported the simple valence description Ta(V), Pd(II) and Ch(2-), and suggested that these compounds are narrow-band-gap degenerate semiconductors [3].

Since their initial synthesis these compounds have been dormant in the literature, but they have received more attention recently, in particular as possible thermoelectric materials, and their electronic

properties have received closer scrutiny. Nakano et al. [12] measured single crystal samples in efforts to explore whether these compounds were potential excitonic insulators or thermoelectric materials. They deduced that Ta<sub>2</sub>PdSe<sub>6</sub> is in fact metallic with a relatively high thermoelectric power factor because of the low resistivity, while Ta<sub>2</sub>PdS<sub>6</sub> is a narrow band gap semiconductor, as originally proposed, with a relatively high thermoelectric power factor because of the higher Seebeck coefficient than in Ta<sub>2</sub>PdSe<sub>6</sub>, arising from a small band gap [12]. Evidently Ta<sub>2</sub>PdS<sub>6</sub> is close to the metallic regime because intercalation of the Lewis base ethylenediamine into Ta<sub>2</sub>PdS<sub>6</sub> was shown to induce superconductivity with a critical temperature *T*<sub>c</sub> of 4.5 K [13]. Since then, further studies have reported pressure-induced superconductivity in Ta<sub>2</sub>PdSe<sub>6</sub> above a pressure of 18.3 GPa with *T*<sub>c</sub> up to 2.8 K [14], an ultrahigh photoconductivity (an increase in electrical conductivity under illumination) and band gap tuneability of exfoliated Ta<sub>2</sub>PdS<sub>6</sub> crystals [15], and giant Peltier conductivity in Ta<sub>2</sub>PdSe<sub>6</sub> [16]. The electronic structures of Ta<sub>2</sub>PdS<sub>6</sub> and Ta<sub>2</sub>PdSe<sub>6</sub> appear in the Materials Project [17,18] (mp-8435 from database version v2022.10.28), which predicts very similar band structures and predicts both compounds to be metallic or close to it. For Ta<sub>2</sub>PdS<sub>6</sub> this prediction is fairly consistent with the experimental measurements which indicate a narrow band gap [12,15]. The calculated band structure suggests that reductive intercalation to raise the Fermi-level in Ta<sub>2</sub>PdS<sub>6</sub> would likely result in metallic behaviour. The observed metallic behaviour of the selenide presumably arises from the higher-lying selenide-based bands which close the small band gap evident in the sulfide.

Here we present two new phases NaTa<sub>2</sub>PdS<sub>6</sub> and KTa<sub>2</sub>PdS<sub>6</sub>,

\* Corresponding author.

E-mail address: [simon.clarke@chem.ox.ac.uk](mailto:simon.clarke@chem.ox.ac.uk) (S.J. Clarke).<https://doi.org/10.1016/j.jssc.2023.124012>

Received 6 February 2023; Received in revised form 17 March 2023; Accepted 26 March 2023

Available online 30 March 2023

0022-4596/© 2023 The Authors. Published by Elsevier Inc. This is an open access article under the CC BY license (<http://creativecommons.org/licenses/by/4.0/>).

synthesised as bulk phases using topochemical intercalation and characterised using high resolution PXRD and SQUID magnetometry. The intercalation results in subtle changes compared to the host and here we compare these reduced phases with the starting material  $\text{Ta}_2\text{PdS}_6$ .

## 2. Experimental

### 2.1. Synthesis

All syntheses were carried out in a Glovebox Technology argon-filled dry glove box with an  $\text{O}_2$  content below 1 ppm or on a Schlenk line. Polycrystalline samples of  $\text{Ta}_2\text{PdS}_6$  were synthesised by grinding together tantalum powder (Alfa Aesar; 99.97%), palladium powder (Alfa Aesar; 99.95%) and sulfur powder (Alfa Aesar; 99.999%) in stoichiometric amounts using an agate pestle and mortar until homogeneous. The mixture was then sealed inside an evacuated silica tube and heated at  $450^\circ\text{C}$  for 12 h, then at  $700^\circ\text{C}$  for 24 h (ramping rate from  $450^\circ\text{C}$  of  $5^\circ\text{C min}^{-1}$ ) before being allowed to cool at the natural rate of the furnace.

Sodium and potassium intercalates were synthesised by adding  $\text{Ta}_2\text{PdS}_6$  powder to a Schlenk tube under argon, along with a magnetic stirrer bar and a stoichiometric amount of Na or K metal (Sigma Aldrich; 99%) to give the target phases  $\text{ATa}_2\text{PdS}_6$  ( $A = \text{Na}, \text{K}$ ). Approximately  $10\text{ cm}^3$  of ammonia was condensed over the reagents using a Schlenk line connected to a cylinder of ammonia (BOC; 99.98%) and with the Schlenk tube cooled to approximately  $-78^\circ\text{C}$  in a bath of isopropanol and dry ice. The suspension was left to stir until all the ammonia had evaporated, then the remaining solid was dried under dynamic vacuum for 20 min (Caution: ammonia is volatile and toxic. The synthesis was performed in a fume hood and at all times the liquid-ammonia-containing vessel was linked to a mercury bubbler to avoid pressures exceeding 1 bar in the reaction vessel).

### 2.2. Diffraction measurements

Laboratory Powder X-ray Diffraction (PXRD) data were collected using a Bruker D8 Advance Eco diffractometer ( $\text{Cu K}\alpha$  radiation) in order to follow the reactions during the high temperature synthesis and the subsequent intercalation steps. For detailed structure refinements of the products, data were collected on beamline I11 [19] at the Diamond Light Source, UK with 1.5 min scans using the multi-angle MYTHEN Position Sensitive Detector (PSD), using Si-calibrated  $0.82\text{ \AA}$  X-rays. Refinements of the structural models against the diffraction data was carried out using the TOPAS Academic V6 software [20].

### 2.3. Magnetometry

Magnetic susceptibility measurements were made using a Quantum Design MPMS-3 SQUID magnetometer. Accurately weighed samples of around 30 mg were loaded into gelatin capsules, which were secured inside plastic straws which were loaded into the instrument. Zero-field-cooled (ZFC) measurements were carried out in fields of 3 T and 4 T. Low field ZFC measurements were carried out at 10 Oe down to 2 K to check for a possible superconducting transition.

## 3. Results and discussion

### 3.1. Structural refinement

The PXRD patterns of both the Na and K intercalates showed obvious shifts in the diffraction peaks compared with the parent phase  $\text{Ta}_2\text{PdS}_6$ , as shown in Fig. 1. The patterns could be well indexed using the auto-indexing routines in the TOPAS Academic V6 software [20], to monoclinic unit cells:  $a = 8.1366(7)\text{ \AA}$ ,  $b = 3.2876(1)\text{ \AA}$ ,  $c = 15.3279(3)\text{ \AA}$ ,  $\beta = 97.407(2)^\circ$  for  $\text{NaTa}_2\text{PdS}_6$  and  $a = 8.3845(3)\text{ \AA}$ ,  $b = 3.2955(1)\text{ \AA}$ ,  $c = 16.7416(8)\text{ \AA}$ ,  $\beta = 86.339(3)^\circ$  for  $\text{KTa}_2\text{PdS}_6$ . These parameters give a 17.3% increase in unit cell volume for the sodium intercalate and a

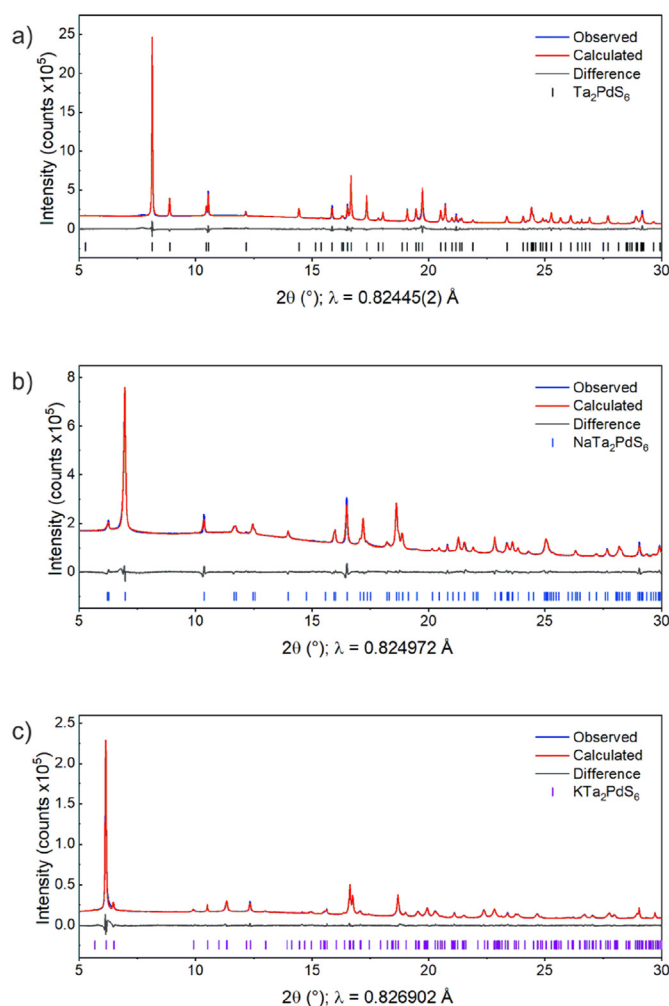


Fig. 1. Rietveld refinements against PXRD patterns of a)  $\text{Ta}_2\text{PdS}_6$ , b)  $\text{NaTa}_2\text{PdS}_6$  and c)  $\text{KTa}_2\text{PdS}_6$  collected at 300 K using the PSD detector on the I11 diffractometer.  $R_{\text{wp}} = 2.99\%$ ,  $2.25\%$  and  $3.67\%$  respectively. See Table S1.

33.2% increase for the potassium intercalate.

To solve the structures of the intercalates, the structure of the parent  $\text{Ta}_2\text{PdS}_6$  phase, was adapted to the new unit cells in a way that replicated the relative atomic positions and bond lengths within the layers in  $\text{Ta}_2\text{PdS}_6$ , thus assuming a topochemical intercalation between these layers. After successful refinement of the Ta, Pd and S positions which dominate the scattering, additional interstitial scattering centres were identified and added to the structural model as the intercalated alkali metal ions using a single site at approximately  $(1/3, 0, 1/8)$  in both compounds. Since this site produces four atoms in the unit cell (i.e. two A ions per formula unit), but a maximum of only two atoms per unit cell is possible due to the stoichiometry of the reaction, the occupancy of the A site was also refined, and the values obtained reflected the stoichiometry of the reaction within the uncertainty in the refinement. To generate the final structural model all atomic positions were refined simultaneously. The increases in interlayer spacing relative to the parent phase are  $0.926\text{ \AA}$  and  $1.868\text{ \AA}$  for the sodium and potassium intercalates respectively, which suggests no co-intercalation of  $\text{NH}_3$  occurred during the reaction based on the larger cell expansions found in such co-intercalates, for example the lithium and ammonia co-intercalates of  $\text{FeSe}$  and  $\text{Bi}_2\text{Se}_3$  in which the interlayer spacings expand by  $2.40\text{ \AA}$  and  $2.72\text{ \AA}$  respectively [11,21]. Structural parameters of both models are given in Tables 1 and 2, and visual representations are given in Fig. 2.

In  $\text{NaTa}_2\text{PdS}_6$ , sodium is found to occupy a 7-coordinate monocapped distorted triangular prism with an average Na–S bond length of  $2.90(1)$

**Table 1**

Refinement parameters from the PXRD pattern of NaTa<sub>2</sub>PdS<sub>6</sub> collected at 300 K using the PSD detector on the I11 beamline.

NaTa <sub>2</sub> PdS <sub>6</sub> Z = 2, RMM = 683.70 g mol <sup>-1</sup>						
Diffractometer	I11 (PSD)					
Wavelength (Å)	0.824972					
Temperature (K)	300					
Space group	I2/m (12)					
a (Å)	8.1366(7)					
b (Å)	3.2876(1)					
c (Å)	15.3279(3)					
β (°)	97.407(2)					
V (Å <sup>3</sup> )	406.60(1)					
Atom	Site	x	y	z	Occ	U <sub>iso</sub> (Å <sup>2</sup> )
Ta	4i	0.3058(2)	0	0.6362(1)	1	0.0125(1)
Pd	2a	0	0	0	1	0.0124(11)
S1	4i	0.7891(7)	0.5	0.4849(5)	1	0.0134(11)
S2	4i	0.3955(8)	0	0.8019(4)	1	0.0134(11)
S3	4i	0.5458(9)	0.5	0.6564(4)	1	0.0134(11)
Na	4i	0.3530(19)	0.5	0.1447(10)	0.53(2)	0.0052(72)

**Table 2**

Refinement parameters from the PXRD pattern of KTa<sub>2</sub>PdS<sub>6</sub> collected at 300 K using the PSD detector on the I11 beamline.

KTa <sub>2</sub> PdS <sub>6</sub> Z = 2, RMM = 699.80 g mol <sup>-1</sup>						
Diffractometer	I11 (PSD)					
Wavelength (Å)	0.826902					
Temperature (K)	300					
Space group	I2/m (12)					
a (Å)	8.3845(3)					
b (Å)	3.2955(1)					
c (Å)	16.7416(8)					
β (°)	86.339(3)					
V (Å <sup>3</sup> )	461.65(3)					
Atom	Site	x	y	z	Occ	U <sub>iso</sub> (Å <sup>2</sup> )
Ta	4i	0.3057(3)	0	0.6410(1)	1	0.0017(9)
Pd	2a	0	0	0	1	0.0136(15)
S1	4i	0.793(14)	0.5	0.4640(7)	1	0.0062(18)
S2	4i	0.3873(13)	0	0.7868(6)	1	0.0062(18)
S3	4i	0.5331(15)	0.5	0.6371(7)	1	0.0062(18)
K	4i	0.3623(20)	0.5	0.1141(9)	0.54(2)	0.0220(85)

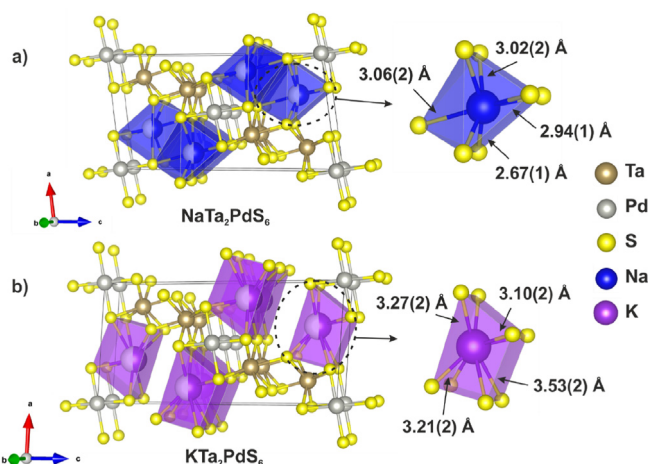


**Fig. 2.** Crystal structures of **a)** NaTa<sub>2</sub>PdS<sub>6</sub> and **b)** KTa<sub>2</sub>PdS<sub>6</sub>. M (M = Na, K) coordination environments and M – S bond lengths are given on the right.

Å, which is comparable to the Na–S bond length in ambient temperature NaTiS<sub>2</sub> of 2.90 Å, where Na occupies a distorted triangular antiprism [22]. In the potassium intercalate, K occupies a distorted square prismatic 8-coordinate site and has an average K–S bond length of 3.28(1) Å,

which is in agreement with the K–S bond length in KCu<sub>4</sub>S<sub>3</sub> of 3.35 Å, in which K occupies an 8-coordinate regular square prismatic site [23]. Bond valence sums of Na and K in their respective intercalates were calculated to be 1.28 and 1.19 respectively [24]. Four alkali metal positions are generated in the unit cell with refined occupancies of 0.53(2) and 0.54(2) for Na and K respectively, to give overall stoichiometries of Na<sub>1.06</sub>Ta<sub>2</sub>PdS<sub>6</sub> and K<sub>1.08</sub>Ta<sub>2</sub>PdS<sub>6</sub>. The occupancies are within 2σ of 0.5, the maximum theoretical occupancy from the reaction stoichiometry of ATa<sub>2</sub>PdS<sub>6</sub>. Attempts to insert larger amounts of the alkali metals resulted in no further change of lattice parameters and a lowering of the crystallinity suggesting that ATa<sub>2</sub>PdS<sub>6</sub> are the limiting compositions using this synthetic route.

Although there are clear similarities between the Na and K intercalates of Ta<sub>2</sub>PdS<sub>6</sub>, both intercalated atoms occupy different co-ordination environments as a consequence of their different sizes. The two different environments arise from subtle structural differences in the relative arrangement of the Ta–Pd–S layers. Although the arrangement of Ta, Pd and S relative to one another within each layer remains essentially unchanged upon intercalation, the relative offset of these layers changes with the size of the intercalated species. Table 3 gives the magnitude of the vectors and angles shown in Fig. 3. The change in φ shows the degree of relative layer ‘sliding’ that has taken place, whilst the interlayer separation (IS) highlights how much the layers move apart perpendicular to one another. Both are important in determining the coordination environment of the intercalated metal and is presumably driven by the size and co-ordination requirements of the intercalated species. A comparison of lattice parameters for both intercalates and the starting material is given in Table 4.

Analysis of the bond lengths of Ta<sub>2</sub>PdS<sub>6</sub> and both intercalates, given in Table 4, shows lengthening of the Ta–S bonds in NaTa<sub>2</sub>PdS<sub>6</sub> and KTa<sub>2</sub>PdS<sub>6</sub> relative to Ta<sub>2</sub>PdS<sub>6</sub>, which is consistent with the reduction of Ta(V). Subtle lengthening of the Pd–S bonds is also observed, and could indicate partial reduction of Pd(II) due to the well-mixed Ta 5 d and Pd 4 d orbitals at the Fermi Level as indicated by the band structure calculations given by the Materials Project [17,18]. The bond valence sum of Ta in Ta<sub>2</sub>PdS<sub>6</sub> was calculated to be 5.27. Values of 4.47 and 4.73 were calculated for Na and K intercalates respectively, supporting the reduction of Ta upon intercalation.

From the refined structural model, the alkali metal ions statistically occupy half of the available sites. The nearest-neighbour and next-nearest-neighbour A–A distances are denoted by (A–A)<sub>NN</sub> and (A–A)<sub>NNN</sub> respectively in Fig. 4. In the sodium intercalate, (Na–Na)<sub>NN</sub> = 3.29(1) Å and (Na–Na)<sub>NNN</sub> = 4.17(3) Å, and in the potassium case (K–K)<sub>NN</sub> = 3.30(1) Å and (K–K)<sub>NNN</sub> = 5.54(1) Å. Given that the diameter of a K<sup>+</sup> ion is approximately 3.30 Å [25], we propose that occupied potassium sites and vacancies are ordered along the 1-D chains which run parallel to the b-axis, with potassium occupying alternate sites. We propose that the in-chain ordering of potassium ions and vacancies is not coherent between layers and this accounts for the average occupancy of 0.5 over these potassium sites observed in the refinement of the structure against the powder diffraction data. Due to the structural similarities between the two intercalates, we assume the sodium ions order in the same fashion. Although the diameter of Na<sup>+</sup> is 2.52 Å [25] and sodium could, in principle, occupy adjacent sites, the Na–Na distance in NaTiS<sub>2</sub> of 3.49 Å [22] is slightly larger than the nearest neighbour distance described

**Table 3**

Vectors (a–c), (a+c)/2, and the angle between them (φ), shown in Fig. 3, of Ta<sub>2</sub>PdS<sub>6</sub> and its intercalates. IS is the interlayer separation, given by the perpendicular distance between the (a–c) vector and the origin.

	Ta <sub>2</sub> PdS <sub>6</sub>	NaTa <sub>2</sub> PdS <sub>6</sub>	KTa <sub>2</sub> PdS <sub>6</sub>
(a–c) (Å)	18.2140(2)	18.2595(7)	18.2388(9)
(a+c)/2 (Å)	5.8928(2)	8.2015(7)	9.5984(9)
φ (°)	79.901(1)	55.696(3)	53.150(3)
IS (Å)	5.802	6.775	7.681



**Table 4**Comparison of lattice parameters and select bond lengths of Ta<sub>2</sub>PdS<sub>6</sub>, NaTa<sub>2</sub>PdS<sub>6</sub> and KTa<sub>2</sub>PdS<sub>6</sub>.

	Ta <sub>2</sub> PdS <sub>6</sub>	NaTa <sub>2</sub> PdS <sub>6</sub>	KTa <sub>2</sub> PdS <sub>6</sub>
<i>a</i> (Å)	9.9420(1)	8.1366(7)	8.3845(3)
<i>b</i> (Å)	3.2735(3)	3.2876(1)	3.2955(1)
<i>c</i> (Å)	11.6826(1)	15.3279(3)	16.7416(8)
$\beta$ (°)	114.525(1)	97.407(2)	86.339(3)
Volume (Å <sup>3</sup> )	345.91(1)	406.60(1)	461.65(3)
Space group	<i>I</i> 2/ <i>m</i>	<i>I</i> 2/ <i>m</i>	<i>I</i> 2/ <i>m</i>
Ta–S1 (Å)	2.494(3)	2.523(6)	2.523(9)
Ta–S2 (Å)	2.487(3)	2.586(6)	2.533(6)
Ta–S3 (Å)	2.483(3)	2.540(6)	2.528(9)
(Ta–S) <sub>average</sub> (Å) <sup>a</sup>	2.488	2.555	2.529
Pd–S1 (Å)	2.346(4)	2.393(6)	2.38(1)
Pd–S3 (Å)	2.336(4)	2.378(7)	2.36(1)

<sup>a</sup> This value was calculated from the weighted average Ta–S distance, individual values all increase at the 3 $\sigma$  level following intercalation.

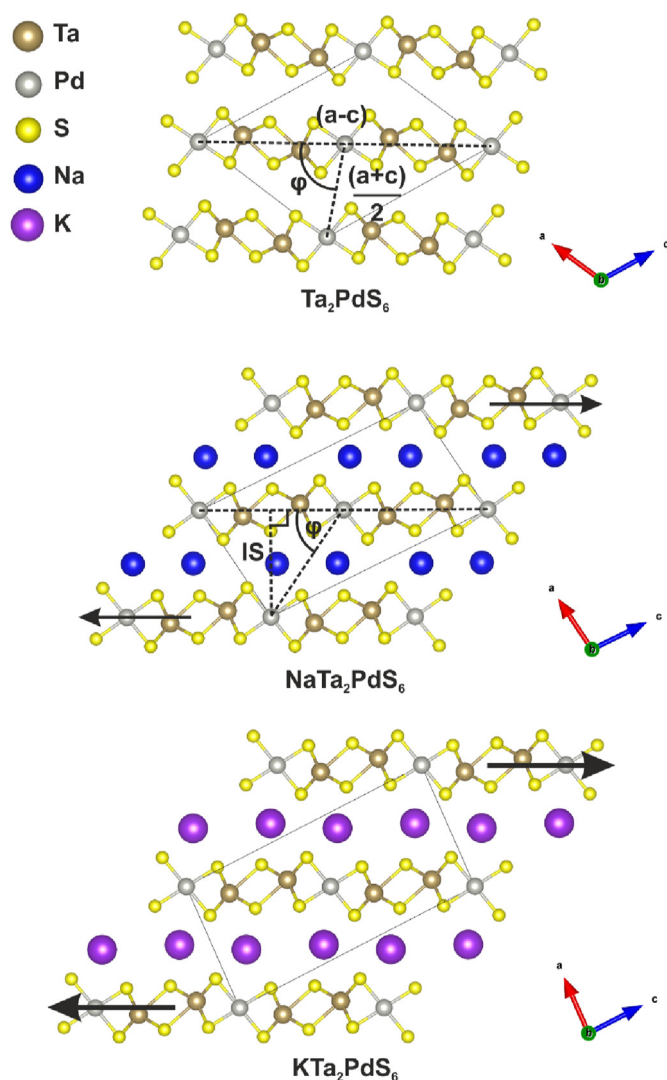


**Fig. 3.** Structural models of Ta<sub>2</sub>PdS<sub>6</sub>, NaTa<sub>2</sub>PdS<sub>6</sub> and KTa<sub>2</sub>PdS<sub>6</sub>. The size of the black arrows reflects the magnitude of the layer offset upon intercalation. Vectors (*a*–*c*), (*a*+*c*)/2, the angle between them ( $\varphi$ ) and the interlayer separation (IS) shows the degree of structural variation. Values are given in Table 3.

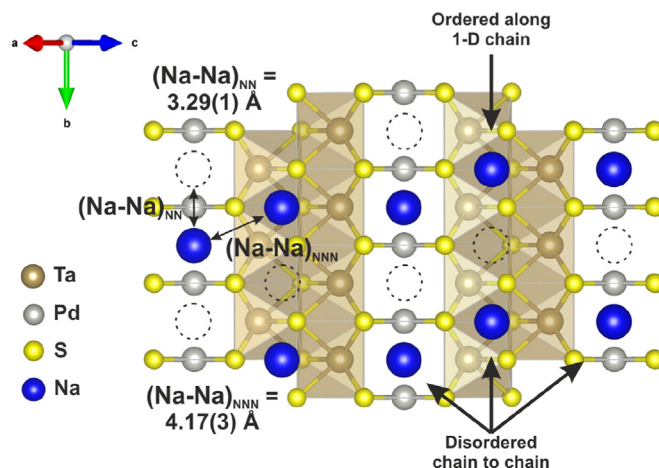


**Fig. 4.** Proposed ordering of Na atoms between the transition metal chalcogenide layers in NaTa<sub>2</sub>PdS<sub>6</sub>, projected along the stacking direction. The interatomic distances between adjacent and diagonal Na atoms are denoted by (Na–Na)<sub>NN</sub> and (Na–Na)<sub>NNN</sub> respectively. Dashed circles represent empty Na sites in this model.

above. As noted above, attempts were made to insert more sodium (or potassium) using a higher reaction stoichiometry but yielded the same phases reported here with 50% occupancy of the available alkali metal sites, which may indicate that it is electrostatically unfavourable for sodium ions to occupy nearest neighbour sites in the chains.

#### 4. Magnetometry

Ambient temperature magnetisation isotherms measured using SQUID magnetometry (Fig. S1) reveal that the parent and intercalate compounds are bulk diamagnets. At low fields both isotherms reveal positive magnetic susceptibilities from 0 to 1 T and this is indicative of a minuscule adventitious ferromagnetic impurity. The susceptibility was determined as a function of temperature by performing measurements at two fields above the saturation field of the ferromagnetic impurity.

Subtraction of the magnetisation vs temperature curves measured at 3 T from those measured at 4 T for Ta<sub>2</sub>PdS<sub>6</sub>, NaTa<sub>2</sub>PdS<sub>6</sub> and KTa<sub>2</sub>PdS<sub>6</sub> eliminates the effect of the minuscule ferromagnetic impurity and gives the intrinsic susceptibility which is found to be temperature independent. Fig. 5 shows a 55% and 37% reduction in the diamagnetic susceptibility, from  $-9.84(8) \times 10^{-5} \text{ emu mol}^{-1}$  in Ta<sub>2</sub>PdS<sub>6</sub> to  $-4.42(7) \times 10^{-5} \text{ emu mol}^{-1}$  in NaTa<sub>2</sub>PdS<sub>6</sub> and  $-6.24(7) \times 10^{-5} \text{ emu mol}^{-1}$  in KTa<sub>2</sub>PdS<sub>6</sub>, upon intercalation of Na and K respectively. The calculated core diamagnetism (using standard tables [26]) for Ta<sub>2</sub>PdS<sub>6</sub> is  $-2.33 \times 10^{-4} \text{ emu mol}^{-1}$ . The observation of a net diamagnetism is smaller in value than the calculated core diamagnetism is consistent with opposing temperature independent core diamagnetism and additional paramagnetic contributions. This suggests that there is a small-temperature independent paramagnetism (TIP) in the parent narrow band gap semiconductor Ta<sub>2</sub>PdS<sub>6</sub> and the injection of electrons from the intercalated Na or K to increase the density of states at the Fermi Level leads to an increased paramagnetism which we presume to be the Pauli paramagnetism expected for a metallic state resulting from the intercalation, which is consistent with the computed band structure and density of states [17,18]. These intercalates are electronically comparable to Ta<sub>2</sub>PdSe<sub>6</sub>, which is also metallic and isostructural to Ta<sub>2</sub>PdS<sub>6</sub>, and has potential applications as a thermoelectric material. Low field ZFC measurements down to 2 K did not reveal any superconducting transition in either intercalate.

#### 5. Conclusions

We have successfully synthesised and characterised the phases NaTa<sub>2</sub>PdS<sub>6</sub> and KTa<sub>2</sub>PdS<sub>6</sub>, synthesised by the intercalation of Ta<sub>2</sub>PdS<sub>6</sub>

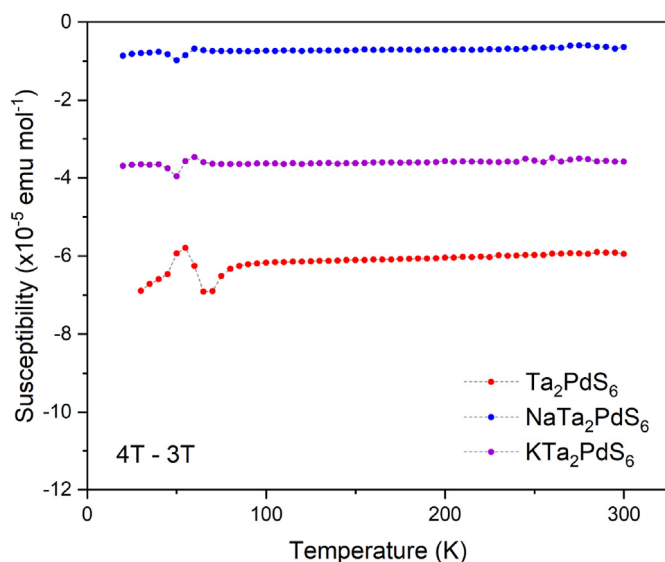


**Fig. 5.** Corrected molar susceptibility vs temperature curves of  $\text{Ta}_2\text{PdS}_6$  (red) and  $\text{NaTa}_2\text{PdS}_6$  (blue) and  $\text{KTa}_2\text{PdS}_6$  (purple), calculated by subtraction of the data points collected at 3 T from those collected at 4 T at each temperature. The kinks observed at approximately 50 K are artifacts due to the presence of small amounts of  $\text{O}_2$  in the magnetometer as shown in Fig. S2.

using alkali metals ( $A = \text{Na}, \text{K}$ ) dissolved in ammonia. The transition metal sulfide layers remain intact in this process, although large unit cell expansions of 17.3% and 33.2% for  $A = \text{Na}$  and  $\text{K}$  respectively, are observed. The relative offset of the layers perpendicular to the stacking direction increases with the size of the intercalated ions and their coordination requirements.  $\text{Na}$  is found to occupy 7-coordinate monocapped triangular prisms with an average  $\text{Na-S}$  bond length of 2.90(1) Å, whilst  $\text{K}$  occupies an 8-coordinate site with an average  $\text{K-S}$  bond length of 3.28(1) Å. SQUID magnetometry shows that both intercalates are diamagnetic, but show a significant reduction in the diamagnetic susceptibility due to the enhancement of temperature independent paramagnetism by injection of electrons from  $\text{Na}$  or  $\text{K}$ , to increase the density of states at the Fermi Level. This work demonstrates alternative routes to synthesising new functional materials, such as potential superconductors or thermoelectric materials.

#### CRediT authorship contribution statement

**P.A. Hyde:** Formal analysis, Writing – original draft. **S.J. Clarke:** Conceptualization, Formal analysis.

#### Declaration of competing interest

The authors declare the following financial interests/personal relationships which may be considered as potential competing interests: Simon J Clarke reports financial support was provided by Engineering and Physical Sciences Research Council. Former associate editor of the journal (2012–2019) *SJC*.

#### Data availability

Data will be made available on request.

#### Acknowledgements

We thank: the UK EPSRC (EP/T027991/1, EP/R042594/1) and the Leverhulme Trust (RPG-2018-377) for funding. We thank the Diamond Light Source Ltd (EE18786 and CY25166) for the award of beam time and Dr A. Baker and Dr C. Murray for support on I11.

#### Appendix A. Supplementary data

Supplementary data to this article can be found online at <https://doi.org/10.1016/j.jssc.2023.124012>.

#### References

- [1] P.A. Madden, M. Wilson, 'Covalent' effects in 'ionic' systems, *Chem. Soc. Rev.* 25 (1996) 339–350, <https://doi.org/10.1039/CS9962500339>.
- [2] E.W. Liimatta, J.A. Ibers, Synthesis, structure, and conductivity of the new ternary chalcogenide  $\text{NbPdTe}_5$ , *J. Solid State Chem.* 77 (1988) 141–147, [https://doi.org/10.1016/0022-4596\(88\)90101-6](https://doi.org/10.1016/0022-4596(88)90101-6).
- [3] D.A. Keszler, P.J. Squattrito, N.E. Brese, J.A. Ibers, S. Maoyu, L. Jiaxi, New Layered Ternary Chalcogenides:  $\text{Ta}_2\text{PdS}_6$ ,  $\text{Ta}_2\text{PdSe}_6$ ,  $\text{Nb}_2\text{PdS}_6$ ,  $\text{Nb}_2\text{PdSe}_6$ , *Inorg. Chem.* 24 (1985) 3063–3067, <https://doi.org/10.1021/ic00213a038>.
- [4] D.A. Keszler, J.A. Ibers, Synthesis and structure of a new ternary chalcogenide  $\text{Nb}_3\text{Pd}_{0.72}\text{Se}_7$ ; interrelationships in the packing of prisms and planes, *J. Am. Chem. Soc.* 107 (1985) 8119–8127, <https://doi.org/10.1021/ja00312a053>.
- [5] D.A. Keszler, J.A. Ibers, S. Maoyu, L. Jiaxi, New ternary and quaternary transition-metal selenides: syntheses and characterization, *J. Solid State Chem.* 57 (1985) 68–81, [https://doi.org/10.1016/S0022-4596\(85\)80061-X](https://doi.org/10.1016/S0022-4596(85)80061-X).
- [6] S.A. Sunshine, J.A. Ibers, Structure and Physical Properties of the New Layered Ternary Chalcogenides  $\text{Ta}_2\text{NiS}_6$  and  $\text{Ta}_2\text{NiSe}_6$ , *Inorg. Chem.* 24 (1985) 3611–3614, <https://doi.org/10.1021/ic00216a027>.
- [7] A. Mar, J.A. Ibers, Synthesis, structure, and physical properties of the new layered ternary telluride  $\text{TaPtTe}_5$ , *J. Solid State Chem.* 92 (1991) 352–361, [https://doi.org/10.1016/0022-4596\(91\)90343-G](https://doi.org/10.1016/0022-4596(91)90343-G).
- [8] S.A. Sunshine, J.A. Ibers, Synthesis, structure, and transport properties of  $\text{Ta}_2\text{NiSe}_7$  and  $\text{Ta}_2\text{PtSe}_7$ , *Inorg. Chem.* 25 (1986) 4355–4358, <https://doi.org/10.1021/ic00244a014>.
- [9] E.W. Liimatta, J.A. Ibers, Synthesis, structure, ternary chalcogenide and physical  $\text{NbNiTe}_5$ , *J. Solid State Chem.* 77 (1987) 141–147, [https://doi.org/10.1016/0022-4596\(88\)90101-6](https://doi.org/10.1016/0022-4596(88)90101-6).
- [10] M.S. Whittingham, Electrical energy storage and intercalation chemistry, *Science* 192 4244 (1976) 1126–1127.
- [11] M. Burrell-Lucas, D.G. Free, S.J. Sedlmaier, J.D. Wright, S.J. Cassidy, Y. Hara, A.J. Corkett, T. Lancaster, P.J. Baker, S.J. Blundell, S.J. Clarke, Enhancement of the superconducting transition temperature of  $\text{FeSe}$  by intercalation of a molecular spacer layer, *Nat. Mater.* 12 (2013) 15–19, <https://doi.org/10.1038/nmat3464>.
- [12] A. Nakano, U. Maruoka, F. Kato, H. Taniguchi, I. Terasaki, Room Temperature Thermoelectric Properties of Isostructural Selenides  $\text{Ta}_2\text{PdS}_6$  and  $\text{Ta}_2\text{PdSe}_6$ , *J. Phys. Soc. Jpn.* 90 (2021), 033702, <https://doi.org/10.7566/JPSJ.90.033702>.
- [13] L. Wuming, Z. Benlian, New ethylenediamine-intercalated superconductor New ethylenediamine-intercalated superconductor, *J. Phys.: Conf. Ser.* 969 (2018), 012176, <https://doi.org/10.1088/1742-6596/969/1/012076>.
- [14] H. Yang, Y. Zhou, L. Li, Z. Chen, Z. Zhang, S. Wang, J. Wang, X. Chen, C. An, Y. Zhou, M. Zhang, R. Zhang, X. Zhu, L. Zhang, X. Yang, Z. Yang, Pressure-induced superconductivity in quasi-one-dimensional semimetal  $\text{Ta}_2\text{PdSe}_6$ , *Phys. Rev. Mater.* 6 (2022), 084803, <https://doi.org/10.1103/PhysRevMaterials.6.084803>.
- [15] P. Yu, Q. Zeng, C. Zhu, L. Zhou, W. Zhao, J. Tong, Z. Liu, G. Yang, Ternary  $\text{Ta}_2\text{PdS}_6$  atomic layers for an ultrahigh broadband photoresponsive phototransistor, *Adv. Mater.* 33 (2021), 2005607, <https://doi.org/10.1002/ADMA.202005607>.
- [16] A. Nakano, A. Yamakage, U. Maruoka, H. Taniguchi, Y. Yasui, I. Terasaki, Giant Peltier conductivity in an uncompensated semimetal  $\text{Ta}_2\text{PdSe}_6$ , *J. Phys. Energy* 3 (2021), 44004, <https://doi.org/10.1088/2515-7655/ac2357>.
- [17] J.M. Munro, K. Latimer, M.K. Horton, S. Dwaraknath, K.A. Persson, An improved symmetry-based approach to reciprocal space path selection in band structure calculations, *Npj Comput. Mater.* 2020 6 1 (2020) 1–6, <https://doi.org/10.1038/s41524-020-00383-7>.
- [18] A. Jain, S.P. Ong, G. Hautier, W. Chen, W.D. Richards, S. Dacek, S. Cholia, D. Gunter, D. Skinner, G. Ceder, K.A. Persson, Commentary: the Materials Project: a materials genome approach to accelerating materials innovation, *Apl. Mater.* 1 (2013), 011002, <https://doi.org/10.1063/1.4812323>.
- [19] S.P. Thompson, J.E. Parker, J. Potter, T.P. Hill, A. Birt, T.M. Cobb, F. Yuan, C.C. Tang, Beamline I11 at Diamond: a new instrument for high resolution powder diffraction, *Rev. Sci. Instrum.* 80 (2009) 879, <https://doi.org/10.1063/1.3167217>.
- [20] A.A. Coelho, TOPAS and TOPAS-Academic: an optimization program integrating computer algebra and crystallographic objects written in C++: an, *J. Appl. Crystallogr.* 51 (2018) 210–218, <https://doi.org/10.1107/S1600576718000183>.
- [21] M.E. Kamminga, S.J. Cassidy, P.P. Jana, M. Elgami, N.D. Kelly, S.J. Clarke, Intercalates of  $\text{Bi}_2\text{Se}_3$  studied in situ by time-resolved powder X-ray diffraction and neutron diffraction, *Dalton Trans.* 50 (2021), 11376, <https://doi.org/10.1039/d1dt00960e>.
- [22] R.J. Haange, A.J.A. Bosalberink, G.A. Wiegers, Structures and phase relations for  $\text{NaTiS}_2$  and compounds  $\text{Na}_x\text{TiSe}_2$ , prepared at temperatures of 200–800 degrees C, *Ann. Chim. Fr.* 3 (1978) 201–207, [10.2146/JQUERY.MIN.JS](https://doi.org/10.2146/JQUERY.MIN.JS).
- [23] W. Rüdorff, H.G. Schwarz, M. Walter, Alkalithio- und -selenoverbindungen der Übergangselemente. III. Strukturuntersuchungen an Alkalithiocupraten, *Z. Anorg. Allg. Chem.* 269 (1952) 141–152, <https://doi.org/10.1002/ZAAC.19522690308>.
- [24] I.D. Brown, Recent developments in the methods and applications of the bond valence model, *Chem. Rev.* 109 (2009) 6858–6919, <https://doi.org/10.1021/cr900053k>.
- [25] R.D. Shannon, Revised effective ionic radii and systematic studies of interatomic distances in halides and chalcogenides, *Acta Crystallogr.* 32 (1976) 751.
- [26] G.F. Bain, J.F. Berry, Diamagnetic corrections and pascals's constants, *J. Chem. Educ.* 85 (2008) 532.